

# On stable wrapper-based parameter selection method for efficient ANN-based data-driven modeling of turbulent flows

Hyeongeun Yun, Yongcheol Choi, Youngjae Kim, Seongwon Kang\*  
*Department of Mechanical Engineering, Sogang University, Seoul 04107, Korea*

To model complex turbulent flow and heat transfer phenomena, this study aims to analyze and develop a reduced modeling approach based on artificial neural network (ANN) and wrapper methods. This approach has an advantage over other methods such as the correlation-based filter method in terms of removing redundant or irrelevant parameters even under non-linearity among them. As a downside, the overfitting and randomness of ANN training may produce inconsistent subsets over selection trials especially in a higher physical dimension. This study analyzes a few existing ANN-based wrapper methods and develops a revised one based on the gradient-based subset selection indices to minimize the loss in the total derivative or the directional consistency at each elimination step. To examine parameter reduction performance and consistency-over-trials, we apply these methods to a manufactured subset selection problem, modeling of the bubble size in a turbulent bubbly flow, and modeling of the spatially varying turbulent Prandtl number in a duct flow. It is found that the gradient-based subset selection to minimize the total derivative loss results in improved consistency-over-trials compared to the other ANN-based wrapper methods, while removing unnecessary parameters successfully. For the reduced turbulent Prandtl number model, the gradient-based subset selection improves the prediction in the validation case over the other methods. Also, the reduced parameter subsets show a slight increase in the training speed compared to the others.

## I. INTRODUCTION

While the turbulent flows can be predicted accurately using the Navier-Stokes equation via direct numerical simulation (DNS), a very high computational cost of DNS is quite demanding for most engineering applications. For efficient alternatives such as the Reynolds-averaged Navier-Stokes (RANS), it is often difficult to construct an accurate closure model with a theoretical approach due to the wide range of length and time scales and strong non-linearity among physical parameters [1–3]. Several multi-physics problems such as the two-phase flows and reacting flows have similar issues in closure modeling. In order to relax this issue, there have been various efforts to use an artificial neural network (ANN) for modeling complex non-linear phenomena. ANN is highly flexible and effective in approximating complex physical relationships arising from strong non-linearity and high dimensions without a predefined model and prior knowledge of the underlying physics. While an ANN-based model may suffer from a lack of self-regulation from competing physical effects, successful outcome may be achieved with sufficient provision of the database.

Among numerous ANN-based approaches for turbulence modeling in the literature, a few of them are introduced briefly here. Milano and Koumoutsakos [4] improved prediction of near-wall flow fields through utilization of data-driven modeling of the wall pressure and shear stress, while Bin et al. [5] improved prediction of the near-wall eddy viscosity using progressive machine learning for various types of flow fields. Rather than improving the prediction of specific flow fields, several studies utilized ANN models to improve the accuracy of the turbulence modeling techniques itself. Sarghini et al. [6] proposed an efficient subgrid-scale model for LES using ANNs trained with an LES database. Subel et al. [7] presented data-driven subgrid modeling of the Burgers turbulence for low generalization error via time shifting and transfer learning. RANS modeling error were reduced by Ling et al. [8] through ANN-modeling of Reynolds stress. Finally, Tracey et al. [9] and Volpiani et al. [10] improved the performance of the Spalart-Allmaras model by using ANN-trained source term.

Despite the advantages associated with ANN-based modeling, the high-dimensional nature of turbulence problems make constructing a well-trained ANN-model especially difficult. ANN-based modeling becomes more efficient by reducing the dimensionality of the input space. Janecek et al. [11], Ladha and Deepa [12] argued that increased dimensionality of the input space can make the training data locally sparse and lead to undesirable errors amplified by inter-parameter dependency, ultimately reducing the accuracy of the trained model. From a computational viewpoint, Marsland [13] and Janecek et al. [11] argued that the memory consumption can be very high for a training a model with high dimensionality of the input space. Also, the trained model may show large errors due to overfitting [14].

---

\* Corresponding author, skang@sogang.ac.kr

Therefore, ANN-based modeling of turbulence problems can benefit significantly from systematic dimensionality reduction via primary parameter identification. Consequently, there have been several studies on dimensionality reduction techniques for flow modeling. A few studies [15–17] identified the modeling parameters using a sequential forward selection approach with ANN and Gaussian process for turbulent modeling. Sun et al. [18] identified dominant parameters for the eddy viscosity using the optimal brain surgeon, decision tree, and ReliefF algorithm. Moghaddam and Sadaghiyani [19] extracted new parameters using the convolutional ANN (CNN) from a parameter set for the Reynolds stress. In Isaac et al. [20], a chemistry model for a reacting flow was simplified by reducing the number of transport equations using the principal component analysis (PCA).

In the above literature, dimensionality reduction techniques for data-driven modeling can be classified into two groups, i.e. parameter (or feature) selection and extraction. In parameter selection, a parameter subset is selected from original parameter set in a database. The parameter selection can be further classified into three sub-categories named as the filter, wrapper, and embedded methods ([12, 21], etc.). A filter method evaluates importance of the parameters based on pre-determined discriminating criteria. The Pearson correlation coefficient and information gain are often used for this purpose. A wrapper method selects the parameters based on the accuracy of a trained model. The sequential forward selection (SFS), sequential backward elimination (SBE), and genetic algorithm belong to this category. An embedded method selects the modeling parameters simultaneously with training a model. Parameter selection using L-1 regularization is an example [22, 23]. On the other hand, the parameter extraction recombines and generates a new parameter set optimized for modeling. PCA is a well-known example. It is based on linear decomposition and may have a limitation for non-linear physics. To relax this limitation, Kramer [24] suggested nonlinear PCA based on ANN, which was extended and applied to turbulent combustion [25]. Callaham et al. [26] employed the Gaussian mixture models and sparse PCA for feature extraction in turbulent boundary layer.

For complex physical problems, different approaches are better for different purposes. In some cases, parameter extraction may not be ideal, because the number of involved physical variables is not reduced, although the dimensionality of a model is reduced [27]. It may be difficult to understand physical meaning of recombined modeling parameters [11]. A filter method may have an issue for a large number of physical parameters with overlapping effects. Because of limited consideration of inter-parameter dependency, redundant parameters may not be removed well [28, 29]. Notably, there have been very limited efforts in the literature on a comparative analysis of dimensionality reduction techniques for modeling the flow problems.

The wrapper method has a relatively high computational cost compared to the filter method; however, the method removes the redundant parameters relatively well even when non-linear relationships exist among variety of the input parameters. When the wrapper methods (e.g., SFS and SBE) are combined with ANN, they show improved capability in handling non-linear relationships but issue of inconsistency over selection trials may arise due to the overfitting and random nature of ANN training. Also, the ANN-based wrapper (ANN-wrapper) method may experience increased generalization errors.

In this background, the first objective of the present study is to analyze and compare different ANN-wrapper methods for efficient modeling of turbulent flow problems. The consistency-over-trials (CoT) of different ANN-wrapper methods are analyzed, which was not examined in the previous studies. As the second objective, a novel ANN-wrapper method is proposed to improve the CoT. The following method relies on a new gradient-based subset selection indices which are elaborated upon in Sec. II. Finally, the performance and characteristics of the newly proposed and existing ANN-wrapper methods are examined. The characteristics of different methods are first examined using a manufactured subset selection problem in Sec. III, followed by actual turbulent flow applications in Secs. IV and V.

## II. DATA-DRIVEN MODELING FOR FLOW PROBLEMS AND PARAMETER SELECTION TECHNIQUES

In this section, a data-driven modeling approach for CFD using a reduced parameter subset is introduced. A few ANN-wrapper methods for parameter selection are explained and discussed. Then, a novel method with improved consistency over selection trials is presented.

### A. An approach of data-driven modeling and simulation

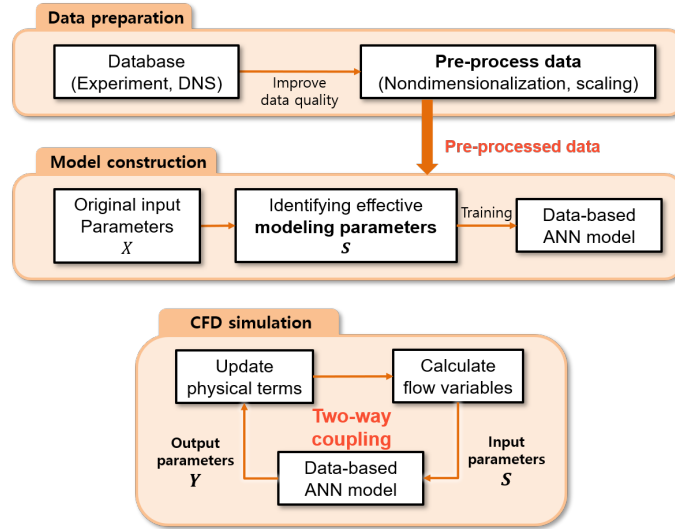


Figure 1: A process diagram of data-driven flow modeling and simulation using ANN and parameter selection.

We consider parameter selection techniques for data-driven modeling of flow problems. Fig. 1 shows a procedure to construct a reduced data-driven ANN model coupled to a flow simulation. This approach is similar to the forward data-driven modeling - one of five categories for data-driven thermal fluid models by Chang and Dinh [30], but the present approach includes a parameter selection (reduction) process for efficient modeling. Each step in Fig. 1 is described below:

1. Data preparation step
  - (a) To collect data from experiments or numerical simulations
  - (b) To pre-process the database (e.g. non-dimensionalization, scaling)
2. Model construction step
  - (a) To determine a parameter subset ( $S$ ) with a reduction technique
  - (b) To train ANN using the pre-processed database and a parameter subset
3. Data-driven simulation step
  - (a) To perform flow simulation using a physics solver coupled with the constructed ANN

### B. Details of ANN-based modeling

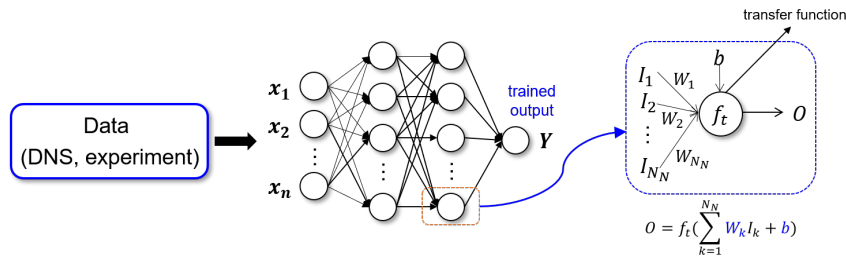


Figure 2: A structure of a fully-connected multi-layer ANN. The symbols  $W_k$ ,  $b$  and  $f_t$  denote the weight, bias and activation function in a neuron operation, respectively.  $N_N$  denotes the number of neurons per hidden layer.

ANN library	Google TensorFlow
Activation function	Hyperbolic tangent
Learning rate	0.0001
Learning algorithm	Adam Kingma and Ba [31]
Loss function	Mean square error

Table I: Hyper-parameters and conditions for training an ANN.

In this study, a fully-connected multi-layer ANN is employed as shown in Fig. 2. Based on ANN, a model function  $f$  can be constructed as

$$Y = f(X) = f(x_1, x_2, \dots, x_{N_x}), \quad (1)$$

where  $Y$  and  $X$  denote the output and input parameter sets, respectively.  $N_x$  is the number (dimension) of the input parameter set. In the present study, the problems with a single output parameter are considered, i.e.  $Y = (y_1)$  and  $X = (x_1, x_2, \dots, x_{N_x})$ . The subscript for  $y$  will be omitted conveniently hereafter. After a parameter selection, a reduced model function  $f_{M_x}$  using a parameter subset will be derived as

$$Y = f_{M_x}(S_{M_x}) = f_{M_x}(x_{s1}, x_{s2}, \dots, x_{M_x}),$$

where  $S_{M_x}$  is a selected parameter subset with the size  $M_x (< N_x)$ .

For a single neuron operation,  $O$  and  $I_k$  represent the output and input values, respectively. A few hyper-parameters and conditions for training ANNs are listed in Table I. Considering the characteristics of the hyperbolic tangent activation function, the database for training is normalized to a range  $[x_{min}^*, x_{max}^*] = [-0.9, 0.9]$  using

$$x^* = x_{min}^* + \frac{x - x_{min}}{x_{max} - x_{min}} (x_{max}^* - x_{min}^*), \quad (2)$$

where the asterisk represents a normalized parameter. The mean square error (MSE) is used as the loss function and written as

$$\text{MSE} = \overline{(Y^{*,ANN} - Y^{*,DB})^2}, \quad (3)$$

where the overbar denotes averaging over the samples in the database. The superscripts  $ANN$  and  $DB$  denote the ANN-predicted and the database values, respectively.

### C. Performance evaluation metrics of reduced model

In the existing wrapper methods (introduced in the next section), a component in the parameter subset is selected from the original (full) parameter set based on a criterion. They often employ either MSE or root mean square error (RMSE) for the purpose. Thus, we can consider the RMSE as a performance evaluation metric (PEM) of a reduced model, i.e.,

$$\text{PEM} - \text{RMSE} = \sqrt{\text{MSE}}. \quad (4)$$

Note that the existing ANN-wrapper methods can be advantageous by using the (nearly) identical indices for the model training, selection criterion, and PEM.

In order to achieve a revised ANN-wrapper method with improved consistency-over-trials (CoT), separate indices for the selection criterion and PEM of a reduced model may be necessary. For the latter, we consider two different PEMs for CoT. The first is the average of  $N$ -highest possibilities among all selected parameters from repeated parameter selections, i.e.,

$$\text{PEM} - \text{CoT1} = \frac{1}{N} \sum_{i=1}^N D(P_N(x_s)), \quad (5)$$

$$P_N(x_s) = \frac{\text{Number of times selecting } x_s}{\text{Number of repeated } S_N \text{ selections}}, \quad (6)$$

where  $x_s$  denotes a (each) parameter selected at least once,  $P_N(x_s)$  is the possibility of selecting  $x_s$  over repeated selections, and  $D$  is the sort function in the descending order. A higher PEM-CoT1 implies that a selected parameter subset has relatively more consistent components over repeated selections. The second PEM for CoT is the highest possibility of selecting a specific subset, i.e.,

$$\text{PEM} - \text{CoT2} = \max \left( \frac{\text{Number of times selecting a } S}{\text{Number of repeated } S_N \text{ selections}} \right), \quad (7)$$

where  $S$  denotes a specific parameter subset. PEM-CoT2 is more strict than PEM-CoT1, thus relatively smaller. Both of them are computed after repeated parameter selections, thus can not be used as the selection criterion.

#### D. ANN-based wrapper methods for parameter selection

##### 1. Sequential forward selection (SFS)

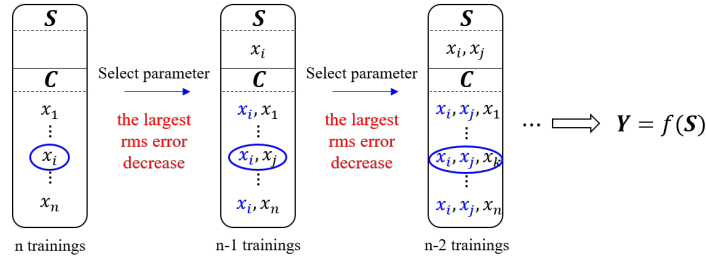


Figure 3: A detailed process of sequential forward selection.

The SFS selects the input parameters sequentially based on a criterion. It was discussed or applied in several previous studies in various fields such as Ladha and Deepa [12], Chandrashekar and Sahin [29], John et al. [32], Kohavi and John [33], Marcano-Cedeno et al. [34]. ANN-based SFS was applied to turbulence modeling [15, 16].

Fig. 3 shows a detailed process of the ANN-based SFS. In order to obtain a parameter subset ( $S_{M_x}$ ), the process starts from an empty set (i.e.  $S_0 = (0)$ ). Then, a group of the candidate subsets ( $C$ ) is generated by adding each parameter to the existing subset ( $S_{n-1}$ ). After training ANNs with all  $C$  members and evaluating the subset selection indices (criteria), the most competitive one is chosen as the new subset ( $S_n$ ). As the subset selection index, the model errors such as the RMSE are used. Based on the RMSE, the objective function of SFS is written as

$$J_{SFS} = \min [\Delta \text{RMSE}] = \min [\text{RMSE}(S_n) - \text{RMSE}(S_{n-1})], \quad (8)$$

where  $\Delta \text{RMSE}$  is negative. This process is iterated until  $|J_{SFS}|$  becomes sufficiently small.

In the literature, it was argued that SFS can produce the optimal parameter subset for ANN-based modeling (e.g. [11, 21, 28, 35]). Compared to the genetic algorithm that searches the optimal subset in a random manner, it is computationally less intensive [36, 37]. In complex inter-parameter relationships, however, it can not remove previously selected parameters that become unnecessary after subsequent selections [12, 29]. Thus, the final subset may be suboptimal. Also, it may produce an inappropriate subset when the model overfitting occurs [29, 33], which will be discussed later.

In the computational viewpoint, the number of ANN trainings to select  $M_x$  parameters from the original  $N_x$  parameters is estimated as

$$N_{\text{training}, SFS} = \sum_{i=1}^{M_x} (N_x - i + 1) = \frac{1}{2} (2M_x N_x + M_x - M_x^2). \quad (9)$$

## 2. Sequential backward elimination (SBE)

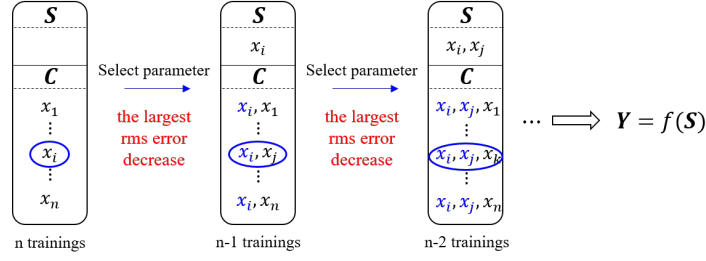


Figure 4: A detailed process of sequential backward elimination. Grey parameters present the removed parameters.

The SBE in previous studies [12, 29, 32, 33] takes a similar approach to the SFS but in the way of reducing dimensionality from the full parameter model, as illustrated in Fig. 4. It starts from the full parameter set ( $S = X$ ) and removes less useful parameters one-by-one. At each iteration, a group of the subsets ( $C$ ) is generated by removing a parameter from the existing subset ( $S_{n+1}$ ). After ANN trainings and error evaluation, new subset ( $S_n$ ) is chosen via the following objective function:

$$J_{SBE} = \min [\Delta \text{RMSE}] = \min [\text{RMSE}(S_n) - \text{RMSE}(S_{n+1})]. \quad (10)$$

While SBE shares several characteristics with SFS, it was mentioned that interaction among the input parameters are better captured than SFS [27, 33], which can be useful for a high-dimensional physics modeling. However, it tends to be computationally more expensive and also prone to an overfitting issue for a high-dimensional parameter set [27, 33].

In the computational viewpoint, the number of ANN trainings to select  $M_x$  parameters from the original  $N_x$  parameters is estimated as

$$N_{\text{training}, SBE} = \sum_{i=1}^{N_x - M_x} (N_x - i + 1) = \frac{1}{2} (N_x^2 + N_x - M_x^2 - M_x). \quad (11)$$

If  $M_x < N_x/2$ , SBE trains a larger number of ANNs than SFS.

## 3. Sequential gradient-based elimination (SGE)

In this study, a new wrapper method is suggested to resolve an issue of the ANN-wrapper methods in the previous sections. A few previous studies [27, 29, 33] mentioned a weakness of SFS and SBE under an overfitting situation of ANN models. In the present study, we observe that SFS and SBE show reduced CoT due to the overfitting and randomness of ANN training, which will be presented in the next sections. To resolve this issue and achieve more stable parameter selection (e.g., higher PEM-CoT1 (Eq. (5)) and PEM-CoT2 (Eq. (7))), we consider two subset selection indices based on the gradient of the model function, i.e.  $\nabla f = \partial f / \partial x_i$ . An idea to remove redundant parameters by minimizing the change of  $\nabla f$  between the new and old subsets is presented here.

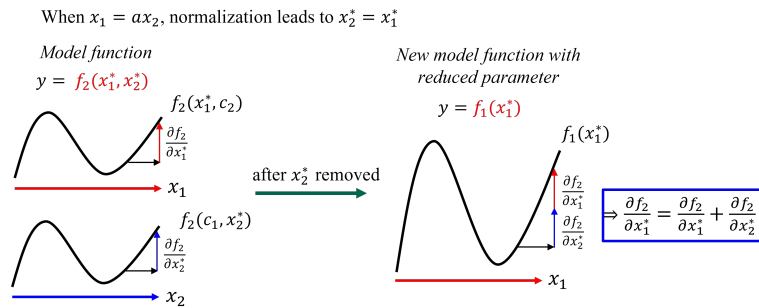


Figure 5: A schematic diagram of the minimum loss of the total derivative to remove redundant parameters.

The first alternative selection index is to minimize the loss of the total derivative between the new ( $S_n$ ) and old ( $S_{n+1}$ ) subsets during a parameter removal. Against  $S_{n+1}$ , it is desirable to preserve the parametric variation of the function with  $S_n$ . In Fig. 5, two parameters  $x_1$  and  $x_2$  satisfy  $x_2 = ax_1$  and have nearly identical effects. After the normalization,  $x_2^* = x_1^*$ . If a model function  $Y^* = f_2(x_1^*, x_2^*)$  is assumed, it leads to  $\frac{\partial f_2}{\partial x_1^*} = \frac{\partial f_2}{\partial x_2^*}$ . Then, the total derivative of  $f_2(x_1^*, x_2^*)$  becomes

$$\frac{df_2}{dx^*} = \frac{\partial f_2}{\partial x_1^*} + \frac{\partial f_2}{\partial x_2^*} = 2 \frac{\partial f_2}{\partial x_1^*} = 2 \frac{\partial f_2}{\partial x_2^*}. \quad (12)$$

When a new model function  $f_1(x_1^*)$  is built by removing  $x_2^*$ ,  $x_1^*$  takes over the effect of  $x_2^*$ . Then, the the total derivative of  $f_1(x_1^*)$  leads to

$$\frac{df_1}{dx^*} = \frac{\partial f_1}{\partial x_1^*} = \frac{\partial f_2}{\partial x_1^*} + \frac{\partial f_2}{\partial x_2^*}. \quad (13)$$

This idea can be extended to an arbitrary input dimension and an objective function of the SGE method to minimize the loss of the total derivative (SGE-TD, hereafter) is written as

$$J_{TD} = \min [\overline{\Delta G_{TD}}] = \min \left[ \left| \sum_{i=1} \frac{\partial f_n}{\partial x_i^*} (S_n) - \sum_{i=1} \frac{\partial f_{n+1}}{\partial x_i^*} (S_{n+1}) \right| \right]. \quad (14)$$

In most problems, the relationship of  $x_2^* = x_1^*$  does not hold exactly but the objective function  $J_{TD}$  can be still useful. A perfectly uncorrelated parameter ( $x_u^*$ ) to  $Y$  also can be removed by  $J_{TD}$ , as  $\frac{\partial f_{n+1}}{\partial x_u^*} \approx 0$  and  $\overline{\Delta G_{TD}} \approx 0$  between  $S_{n+1}$  and  $S_n$  without  $x_u^*$ . If an essential parameter to  $Y$  is removed, the partial derivatives of the trained model can exhibit a random behavior while redistributing its contribution with a limited success, which affects  $\overline{\Delta G_{TD}}$  significantly.

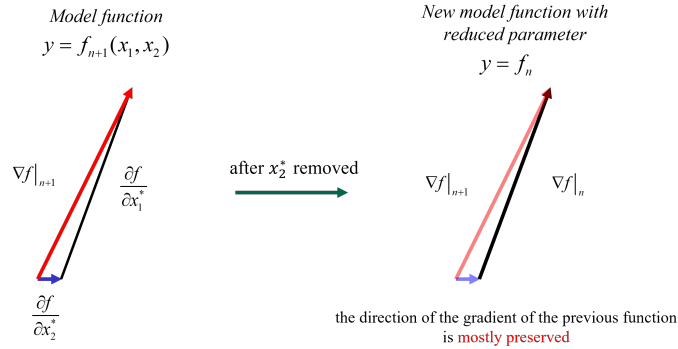


Figure 6: A schematic diagram of the directional consistency of  $\nabla f$  in case of unimportant parameter to  $Y$ .

The second alternative selection index is to preserve the gradient direction between the new and old subsets. As shown in Fig. 6, if a parameter  $x_2$  has a trivial contribution to  $Y$ ,  $\nabla f_n$  and  $\nabla f_{n+1}$  excluding  $x_2$  will be similar. This idea leads to an objective function as

$$J_{DC} = \min \left[ 1 - \frac{|\nabla f_n \cdot \nabla f_{n+1 \rightarrow n}|}{|\nabla f_n| |\nabla f_{n+1 \rightarrow n}|} \right], \quad (15)$$

where  $\nabla f_{n+1 \rightarrow n}$  denotes  $\nabla f_{n+1}$  reduced to  $n$ -dimension by excluding a single component. This aims at preserving the directional consistency of the gradient and called as SGE-DC hereafter.

The SGE methods (SGE-TD and SGE-DC) follow the same procedure as SBE with the different objective function  $J_{TD}$  or  $J_{DC}$ . Under a circumstance of the overfitting, some neuron weights may become excessive during training to keep reducing the RMSE, which increases the sizes of the partial derivatives. The gradient-based indices can impose a penalty in such a case and may improve the CoT compared to SFS and SBE using the RMSE. The partial derivatives of an ANN are computed in a semi-analytic way using a built-in feature of TensorFlow.

Also, it is possible to construct a mixed criterion of  $\overline{\Delta G_{TD}}$  (or  $\overline{\Delta G_{DC}}$ ) and  $\Delta \text{RMSE}$  (in Eq. (10)) to impose both criteria simultaneously, e.g.,

$$J_{mixed} = \min \left[ \alpha_{SGE} \times \frac{\overline{\Delta G_{TD}}}{G_{TD}(X)} + (1 - \alpha_{SGE}) \times \frac{\Delta \text{RMSE}}{\text{RMSE}(X)} \right]. \quad (16)$$

Note that the present study focuses on testing SGE and a test on  $J_{mixed}$  is reserved for a subsequent study.

### III. APPLICATION TO A MANUFACTURED SUBSET SELECTION PROBLEM

In this section, the characteristics of ANN-wrapper methods introduced in the previous section are analyzed using a manufactured subset selection problem. We create an artificial database including a few randomly distributed parameters and derived ones. We examine the performance to remove redundant or irrelevant parameters and select a desirable subset.

#### A. Description of a manufactured problem and parameter set

We consider three independent random parameters ( $x_1$ ,  $x_4$ , and  $x_7$ ) with uniform distributions between 0 and 1. A few other parameters are derived from them using the following equations:

$$\begin{cases} x_2 = x_1^2, & x_3 = -\exp(x_1 - 0.5) \\ x_5 = \exp(x_4), & x_6 = x_4^3 \end{cases} \quad (17)$$

where the first and second rows shows the parameters derived from  $x_1$  and  $x_4$ , respectively. The output parameter  $y$  is defined as

$$y = \frac{x_3 x_4 + (x_2 - x_5) + (x_1 + x_6)}{3}, \quad (18)$$

where  $x_7$  is omitted on purpose and becomes an irrelevant parameter to  $y$ .  $x_i$  are categorized into  $x_1$ -group and  $x_4$ -group. The parameters in each group are co-dependent among themselves.

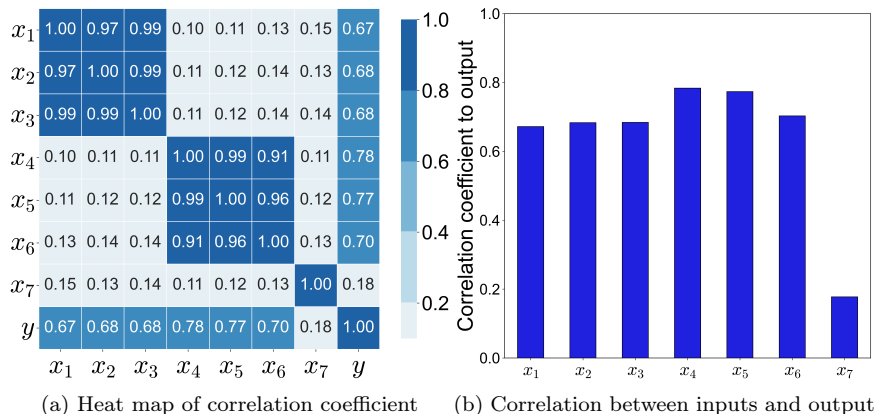


Figure 7: Pearson correlation coefficients of the manufactured problem.

Fig. 7 shows the Pearson correlation coefficients among the parameters. In Fig. 7(a), the heat map shows that the parameters in the same group are relatively highly correlated, denoting that they have similar effects. Fig. 7(b) shows the correlation coefficients between each parameter and the output  $y$ . It shows that all parameters except  $x_7$  have similarly high correlation coefficients with  $y$ . If the filter method ([27, 29, 38]) based on the correlation coefficient is used,  $x_4$  and  $x_5$  must be the first two parameters selected. Selecting two parameters with similar effects is not ideal and leads to a suboptimal subset.

From  $y = f(x_1, \dots, x_7)$ , an ideal subset  $S_2$  is assumed to have one parameter from each group. Such an outcome based on the first two parameters selected for SFS or the last two parameters for SBE and SGE is regarded as a successful selection. This is used to evaluate the CoT of the ANN-wrapper methods in the next section.



## B. Results of dimensionality reduction for manufactured problem

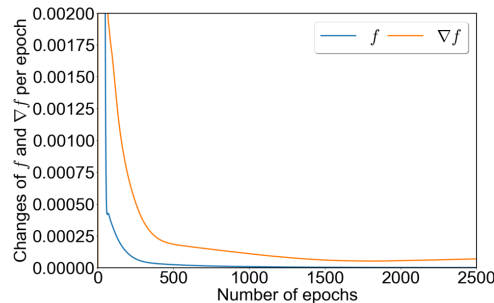


Figure 8: Absolute changes of  $f$  and  $\nabla f$  per epoch averaged over samples for 2L-10N/L ANN for the manufactured problem.

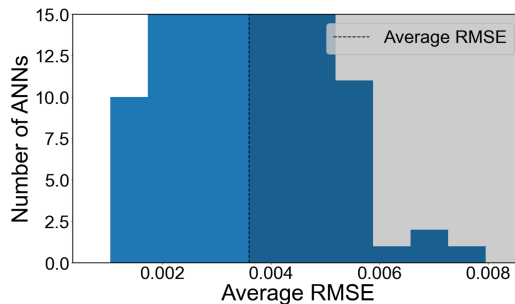


Figure 9: Histogram of the RMSE from 200 trained ANN models for the manufactured problem.

The ANN-wrapper methods introduced in Sec. 2 are applied to the manufactured problem. The number of training epochs is set to 2500 times. To evaluate the success (and failure) rate of each method, the parameter selections are tried for 200 times.

Fig. 8 shows the absolute changes of  $f$  and  $\nabla f$  per epoch averaged over samples for 2L-10N/L (2 layers, 10 neurons/layer) ANN. In Fig. 8, the change of  $\nabla f$  per epoch decreases much more slowly compared to  $f$ . Therefore, at the same training epochs, a relatively larger error may exist in the gradient compared to the function. A large error in the gradient can make the SGE selection inconsistent. For a solution to this issue, we consider that the ANNs with smaller RMSE at the same training epochs also have smaller errors in their gradient. Then, we can train the ANNs multiple ( $N$ ) times and utilize only the ANNs with 50% below-average RMSE (well-trained ANNs, hereafter) during the selection. While this can increase the overall training time by  $N$  times, we found from a test that selecting only the final subset (e.g.  $S_2$ ) using well-trained ANNs similarly improves the success rate (or CoT) of SGE significantly. Then, the increase of the computational cost is minimal. Fig. 9 shows the RMSE histogram from 200 trained ANNs. The case using well-trained ANNs utilizes the ANNs belonging to the left (bright) side of the histogram. To validate the present approach, the results using well-trained ANNs are compared with those using all trained ANNs.

Method	1L-30N/L			2L-10N/L			4L-30N/L		
	S	R	F	S	R	F	S	R	F
SFS	1	0	0	1	0	0	1	0	0
SBE	1	0	0	1	0	0	1	0	0
SGE-TD	0.975	0.025	0	0.99	0.01	0	1	0	0
SGE-DC	0.88	0.12	0	0.995	0.005	0	1	0	0

Table II: The success (S), redundancy (R), and failure (F) rates of  $S_2$  over 200 selection trials using all trained ANNs for the manufactured problem.

Method	1L-30N/L			2L-10N/L			4L-30N/L		
	S	R	F	S	R	F	S	R	F
SFS	1	0	0	1	0	0	1	0	0
SBE	1	0	0	1	0	0	1	0	0
SGE-TD	1	0	0	1	0	0	1	0	0
SGE-DC	1	0	0	1	0	0	1	0	0

Table III: The success (S), redundancy (R), and failure (F) rates of  $S_2$  over 100 selection trials using well-trained ANNs for the manufactured problem.

Tables II and III show the success (S), redundancy (R), and failure (F) rates of  $S_2$  over 100-200 trials of parameter selection using all trained ANNs and well-trained ANNs, respectively. Redundancy means selecting two parameters from a single group. Failure means one of two selected parameters is irrelevant one ( $x_7$ ). When all trained ANNs are used, SFS and SBE produce perfectly successful parameter selection. On the other hand, the two SGE methods show a less success rate for relatively lower hyper-parameters. In contrast, when using well-trained ANNs, the SGE methods also yield perfectly successful parameter selection regardless of hyper-parameters. It is known that  $\nabla f$  is more sensitive to the numerical error than the model function  $f$ . The present results show that SGE is more sensitive than SFS and SBE to the training error of ANN. It is also shown that SGE using  $\nabla f$  can successfully remove redundant and irrelevant parameters. Only the results using well-trained ANNs are presented below.

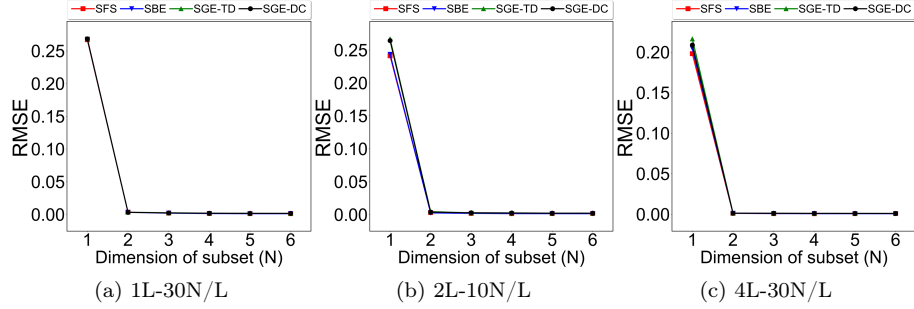


Figure 10: RMSE averaged over trials according to the size of  $S_N$  for the manufactured problem.

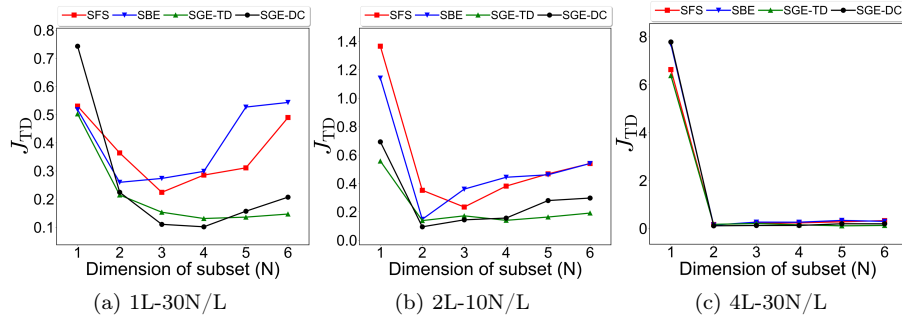


Figure 11:  $J_{TD}$  averaged over trials according to the size of  $S_N$  for the manufactured problem.

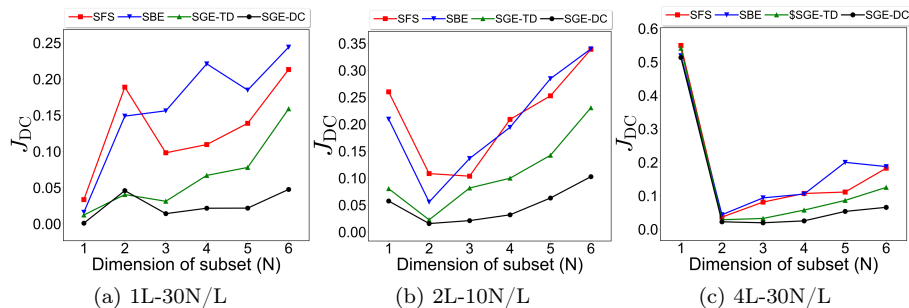


Figure 12:  $J_{DC}$  averaged over trials according to the size of  $S_N$  for the manufactured problem.

Fig. 10 shows the RMSE averaged over trials according to the size of the subset  $S_N$  for each method using well-trained ANNs. The RMSE is minimized from  $S_2$  regardless of hyper-parameters for all methods, including SGEs that do not use the RMSE. Figs. 11 and 12 show  $J_{TD}$  (Eq. (14)) and  $J_{DC}$  (Eq. (15)) averaged over trials according to the size of  $S_N$ . In most cases, SGE-TD shows the lowest  $J_{TD}$  among all methods, and SGE-DC shows the lowest  $J_{DC}$ . The changes of  $J_{TD}$  and  $J_{DC}$  of SFS and SBE look similar to those of SGE, but their convergence looks less clear especially for lower hyper-parameters.

#### IV. DATA-DRIVEN MODELING OF BUBBLE SIZE IN TURBULENT BUBBLY FLOWS IN A PIPE

In this section, the analysis of the ANN-wrapper methods is extended to data-driven modeling for turbulent bubbly flows in a pipe. A data-driven model of the Sauter mean diameter ( $D_{sm}$ ) important in this problem is considered.

##### A. Description of physical problem and data-driven modeling

Turbulent bubbly flows are observed frequently in several engineering problems such as the boilers, heat exchangers, nuclear reactors, and various chemical processes [39]. In engineering applications, an Eulerian-Eulerian approach called as the two-fluid model ([40, 41], etc.) is used widely. In an iso-thermal and low Mach number condition, the governing equations for a RANS simulation are written as

$$\frac{\partial(\alpha_q \rho_q)}{\partial t} + \nabla \cdot (\alpha_q \rho_q \vec{u}_q) = 0, \quad (19)$$

$$\frac{\partial(\alpha_q \rho_q \vec{u}_q)}{\partial t} + \nabla \cdot (\alpha_q \rho_q \vec{u}_q \vec{u}_q) = -\alpha_q \nabla P + \alpha_q \rho_q \vec{g} + \nabla \cdot (\alpha_q \tilde{\tau}_q + \alpha_q \tilde{\tau}_q^t) + \vec{M}_q, \quad (20)$$

where the subscript  $q$  represents either the liquid (L, water) or gas (G, air) phases, respectively. The symbols  $\alpha$ ,  $\rho$ ,  $\vec{u}$ ,  $\tilde{\tau}$  and  $\tilde{\tau}^t$  denote the volume fraction, density, velocity vector, molecular and turbulent stress tensors of a phase, respectively. The symbols  $P$  and  $\vec{g}$  are the pressure and acceleration gravity vector, respectively.  $\vec{M}_q$  includes the interfacial momentum exchange terms such as the drag, shear- and wall-induced lifts, and turbulent dispersion force. Details on their physical models used in this study are found in Ishii and Mishima [40], Kim et al. [41], Ishii and Zuber [42], Sato et al. [43], Tomiyama et al. [44], Kim et al. [45] as summarized in Jung et al. [46]. As noted in Colombo and Fairweather [47], a primary factor to model the interfacial momentum exchange terms is the bubble size called as the Sauter mean diameter ( $D_{sm}$ ). Due to its physical and practical importance, there exist numerous studies (e.g. [48–55], etc.) on its modeling. It is difficult to develop a model predicting the bubble size accurately due to complex interaction between the turbulence and bubbles [56]. Although there have been a few efforts on data-driven modeling such as Shaikh and Al-Dahhan [57], Monrós-Andreu et al. [58] and Ma et al. [59], there exist very limited studies on machine learning for a closure model to simulate a bubbly flow. Recently for turbulent flows in a vertical pipe, Jung et al. [46] presented modeling of  $D_{sm}$  using ANN with experimental database and a closure approach for RANS simulations. Based on this approach, we aim to produce a reduced model for  $D_{sm}$  from the full parameter model of [46].

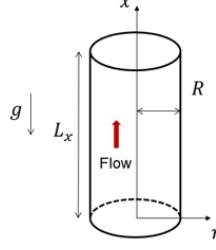


Figure 13: A schematic diagram of a turbulent bubbly flow in a vertical round pipe.

Symbol	$\rho_L, \rho_G / \mu_L, \mu_G$	$u_L, u_G$ (m/s)	$J_L, J_G$ (m/s)	$\alpha_G$
Meaning	Density / Viscosity	Local mean axial velocity	Inlet superficial velocity	Local void fraction
Value	Constants for water and air	0.41-2.795, 0.647-3.098	0.491-2.01, 0.0275-0.321	0.049-0.259

Table IV: Variables in the database of turbulent bubbly flows in a pipe.

There are a few experimental studies on turbulent bubbly flow in vertical pipes ([58, 60–62]) with a schematic diagram in Fig. 13. The data from these studies include a few common variables listed as

- Material properties :  $\rho_G, \rho_L, \mu_G, \mu_L$
- Flow variables :  $u_G, u_L, J_G, J_L, \alpha_G$

The physical meanings and values of these variables are presented in Table IV. A database is built using the results of 15 flow cases in the literature. Further details on the database are available in Jung et al. [46]. We employ the non-dimensionalized  $D_{sm}$  model in [46] as the full parameter model, i.e.,

$$\frac{D_{sm}}{R} = f \left( Re_L, \frac{J_G}{J_L}, \alpha_G, \frac{u_L}{J_L}, \frac{u_G}{J_L} \right), \quad (21)$$

which is regarded as  $Y = f(X)$ . It is noted that  $(\alpha_G, u_L/J_L, u_G/J_L)$  are the Reynolds-averaged spatially varying (local) variables.  $(Re_L, J_G/J_L)$  are the conditions of each flow case.

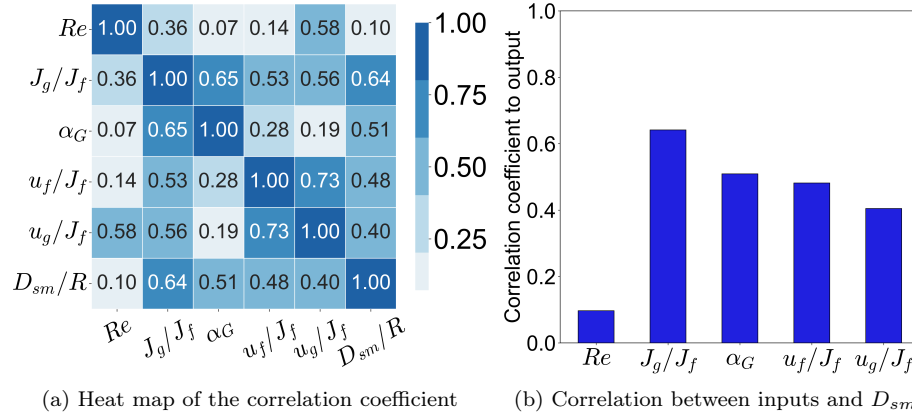


Figure 14: Pearson correlation coefficients of turbulent bubbly flows in a pipe.

Fig. 14 shows the Pearson correlation coefficients among the parameters from the database. In Fig. 14(a), it is shown that relatively strong inter-dependency between  $u_L/J_L$  and  $u_G/J_L$  as well as  $J_G/J_L$  and  $\alpha_G$ . It is anticipated that two-phase velocities are correlated closely. A relatively large gas-phase velocity at the inlet (i.e. a large  $J_G/J_L$ ) leads to an increased void fraction in the downstream. From these, the overlapping effects are assumed inside each pair of  $(u_L/J_L, u_G/J_L)$  and  $(J_G/J_L, \alpha_G)$ . Fig. 14(b) shows that  $D_{sm}$  shows the highest correlation with  $J_G/J_L$  followed by  $\alpha_G$ .

It is noted that this problem has a relatively small number of the parameters and may not be ideal to investigate the effects of dimensionality reduction methods. This database has a range of operating conditions from several accredited sources but the data resolution is rather coarse. Thus, it can be useful to test practical performance of the ANN-wrapper methods including SGE for a sparse database.

### B. Results of dimensionality reduction for $D_{sm}$ model

The ANN-wrapper methods are applied to the full parameter  $D_{sm}$  model (Eq. (21)) to obtain reduced parameter subsets. The number of training epochs is determined using the K-fold technique [63] with 5-fold cross validation [64]. To evaluate the averaged performance and the consistency over selection trials (e.g., PEM-CoT1 and PEM-CoT2), the parameter selections are tried for 20-35 times.

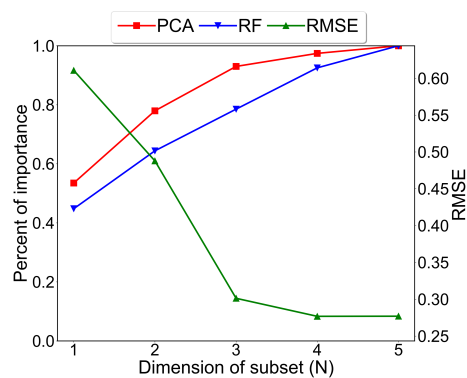


Figure 15: Accumulated feature importance of the RF method and PCA compared with the minimum RMSE (validation) of parameter combinations over the number of components.

To estimate the necessary dimension of a reduced  $D_{sm}$  model, Fig. 15 shows the accumulated feature importance of the random forest (RF) method and PCA over the number of components. The green line shows the minimum RMSE of all parameter combinations with a specific number of input parameters. It is shown that the RF method and PCA needs 3-4 parameters for sufficiently converged ( $> 90\%$  in importance) model prediction, similarly to the RMSE trend. Thus, reduced parameter subsets of 3 parameters (i.e.  $S_3$ ) are considered below.

	1L-30N/L		2L-30N/L		4L-30N/L	
Method	A-T	W-T	A-T	W-T	A-T	W-T
SFS	1	1	0.883	0.889	1	1
SBE	1	1	1	1	1	1
SGE-TD	1	1	1	1	1	1
SGE-DC	1	1	0.994	1	1	1

Table V: PEM-CoT1 of  $S_3$  over 20-35 selection trials using different hyper-parameters for turbulent bubbly flows in a pipe (A-T: all trained ANNs (35), W-T: well-trained ANNs (20)).

	1L-30N/L		2L-30N/L		4L-30N/L	
Method	A-T	W-T	A-T	W-T	A-T	W-T
SFS	1	1	0.657	0.85	1	1
SBE	1	1	1	1	1	1
SGE-TD	1	1	1	1	1	1
SGE-DC	1	1	0.971	1	1	1

Table VI: PEM-CoT2 of  $S_3$  over 20-35 selection trials using different hyper-parameters for turbulent bubbly flows in a pipe (A-T: all trained ANNs (35), W-T: well-trained ANNs (20)).

To examine the CoT of the parameter selection, Tables V and VI show PEM-CoT1 (Eq. (5)) and PEM-CoT2 (Eq. (7)) metrics of  $S_3$  over 20-35 selection trials using different ANN-wrapper methods, hyper-parameters, and trained ANNs. With 2L-30N/L, SFS show relatively low CoT metrics even with well-trained ANNs. The CoT metrics of SGE-DC looks slightly reduced with all trained ANNs but becomes ideal (i.e. 1) with well-trained ANNs. SBE and SGE-TD show the perfect CoT for all cases.

Method	1L-30N/L	2L-30N/L	4L-30N/L
SFS	$Re, J_g/J_f, u_f/J_f$	$Re, J_g/J_f, u_g/J_f$	$Re, J_g/J_f, u_g/J_f$
SBE	$\alpha_G, Re, u_g/J_f$	$\alpha_G, Re, u_g/J_f$	$\alpha_G, Re, u_g/J_f$
SGE-TD	$\alpha_G, Re, u_g/J_f$	$\alpha_G, Re, u_g/J_f$	$\alpha_G, Re, u_f/J_f$
SGE-DC	$\alpha_G, Re, u_g/J_f$	$\alpha_G, Re, u_g/J_f$	$\alpha_G, Re, u_f/J_f$

Table VII: List of 3 parameters with the highest selection possibilities from  $S_3$  over selection trials for turbulent bubbly flows in a pipe.

Table VII show the list of 3 parameters with the highest selection possibilities from  $S_3$ . SFS does not select  $\alpha_G$  that is known to be a primary factor for  $D_{sm}$ . Instead of  $\alpha_G$ , SFS selects  $J_G/J_L$  correlated to  $\alpha_G$ , but  $J_G/J_L$  is not a spatially varying parameter and may be less effective to model  $D_{sm}$ . For all cases, either  $u_f/J_f$  or  $u_g/J_f$  is selected due to their close similarity.

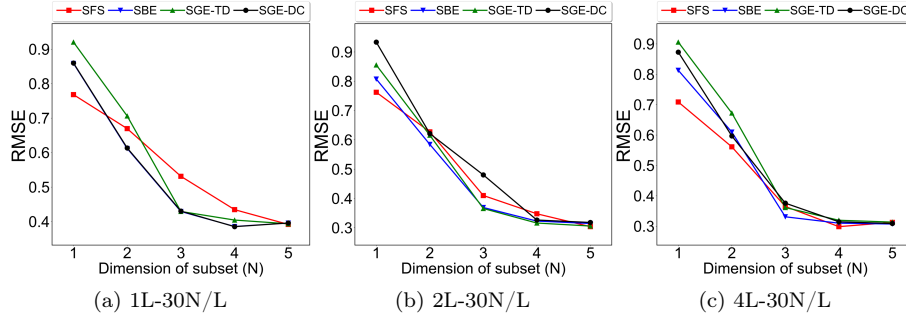


Figure 16: RMSE (validation) averaged over trials according to the size of  $S_N$  for turbulent bubbly flows in a pipe.

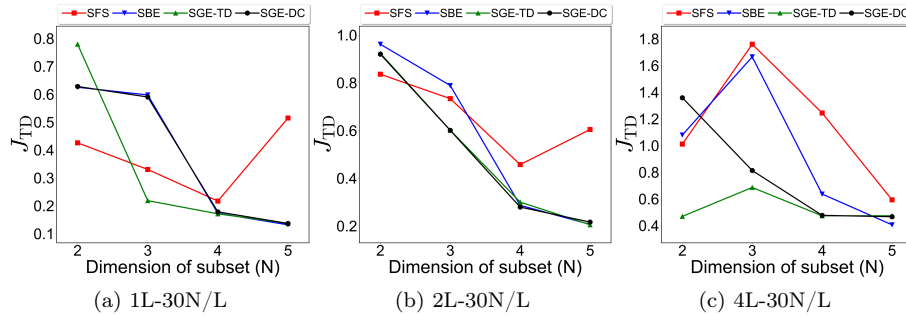


Figure 17:  $J_{TD}$  averaged over trials according to the size of  $S_N$  for turbulent bubbly flows in a pipe.

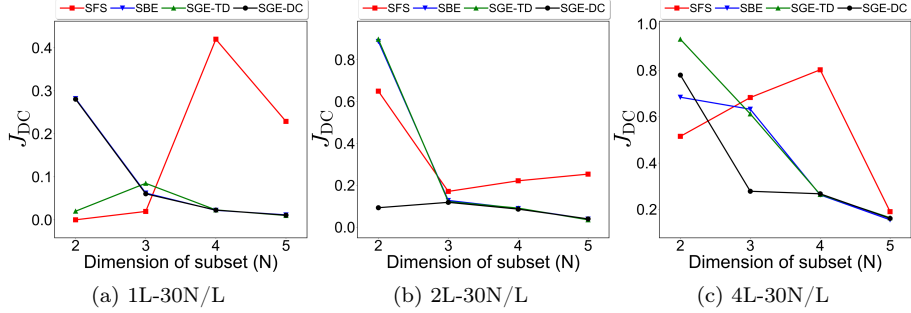


Figure 18:  $J_{DC}$  averaged over trials according to the size of  $S_N$  for turbulent bubbly flows in a pipe.

Fig. 16 shows the RMSE averaged over trials according to the size of the subset  $S_N$  for each method using well-trained ANNs. Figs. 17 and 18 show  $J_{TD}$  and  $J_{DC}$  averaged over trials according to the size of  $S_N$ . Overall trends look similar to those of the manufactured problem. It is shown that the RMSE of SFS is somewhat worse than the others and the SGE methods show the comparable RMSE to SBE.  $J_{TD}$  and  $J_{DC}$  are smallest for the SGE methods.

## V. DATA-DRIVEN MODELING OF TURBULENT PRANDTL NUMBER IN A DUCT FLOW

### A. Description of physical problem and data-driven modeling

The turbulent Prandtl number ( $Pr_t$ ) is an important parameter to predict the heat transfer rate in RANS simulations by relating the turbulent diffusivity ( $\alpha_t$ ) and the turbulent viscosity ( $\nu_t$ ).  $Pr_t$  has been assumed often as a constant based on the Reynolds analogy [65]. For various turbulent flows, however, several previous studies showed that  $Pr_t$  varies significantly over space, e.g., flows around a cylinder [66–68], jet flows [69, 70]. Due to its importance, there are many previous studies on modeling  $Pr_t$  ([71–74], among others). However, there are only limited studies on spatially varying  $Pr_t$  models [75, 76]. Mostly, they employ simple relationships using  $Re$ ,  $Pr$ , the wall distance, and  $\nu_t$  to model only the wall-normal distribution, and the similarity to a DNS result is marginal.

Therefore, the present study aims at addressing this issue by applying the ANN-wrapper method to a DNS database for a turbulent flow inside a duct. The database is obtained from Nam [77], and the problem is briefly introduced. In the domain shown in Fig. 19, the top and bottom walls are heated to a higher temperature which leads to an incompressible flow with forced convection. The Reynolds number based on the wall unit is  $Re_\tau=150$ . To avoid the overfitting issue, the results of  $Pr=0.2, 2.0$  are used for the train data and those of  $Pr=0.7$  are used for the validation data.

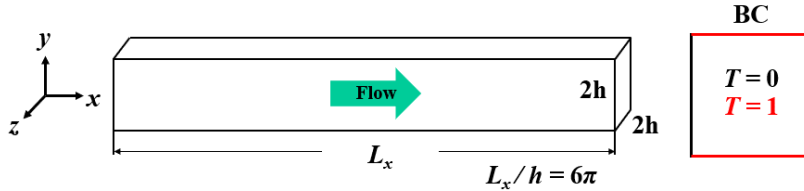


Figure 19: A physical domain of a turbulent flow inside a duct with heat transfer.

On the input parameters for the model  $Pr_t = f(X)$ , a few parameters available from RANS simulations are utilized. We consider a few Galilean-invariant variables derived from the velocity, and pressure, and turbulent kinetic energy (TKE) as well as  $\nu_t$  often used in the previous models. For a high-dimensional database, a few variables in the mean budget equations are also considered, supposing their close relationships to the TKE and temperature variance budget equations that are crucial to turbulent transport. All candidate parameters are listed in Table VIII and the definitions of the mean budget terms are presented in Appendix. The dimension of the full parameter model is 12 that is larger than 5 of the turbulent bubbly flow. This possibly makes achieving a high CoT more difficult. Considering the histogram of the database variables, the following standardization (instead of normalization) is used to pre-process the input and output parameters:

$$x^* = \frac{x - \bar{x}}{\sigma_x}, Y^* = \frac{Y - \bar{Y}}{\sigma_Y}, \quad (22)$$

where  $\sigma$  refers to the standard deviation.

Global parameters	$Pr$	Prandtl number
Local parameters	$\nu_t$	Turbulent viscosity
	$k$	Turbulent kinetic energy
	$\Pi_{MKE}$	Mean pressure transport
	$\varepsilon_{MKE}$	Mean dissipation
	$D_{MKE}$	Mean viscous diffusion
	$\varepsilon_{MTV}$	Mean temperature dissipation
	$D_{MTV}$	Mean molecular diffusion
	$ \partial P/\partial x_i $	Magnitude of pressure gradient
	$ \partial T/\partial x_i $	Magnitude of temperature gradient
	$ \partial k/\partial x_i $	Magnitude of turbulent kinetic energy gradient
	$ S_{ij} $	Magnitude of strain rate tensor

Table VIII: A list of input parameters ( $X$ ) to model the turbulent Prandtl number in a duct.

Fig. 20 shows the Pearson correlation coefficients among the parameters and  $Pr_t$ . A difficulty in modeling spatially varying  $Pr_t$  is conjectured from complicated relationships in Fig. 20(a). Fig. 20(b) shows the correlation coefficients between  $Pr_t$  and input parameters. There are three variables (i.e.  $k$ ,  $\nu_t$  and  $|\partial k/\partial x_i|$ ) with the correlation coefficients of 0.3 or larger to  $Pr_t$ , but overall the correlation coefficients are relatively much smaller compared to the previous two applications. In Fig. 20(a), there are about 10 additional variables with the correlation coefficients of 0.3 or larger to ( $k$ ,  $\nu_t$  and  $|\partial k/\partial x_i|$ ). This implies the complex relationships among the parameters and possibly overlapping effects among them.

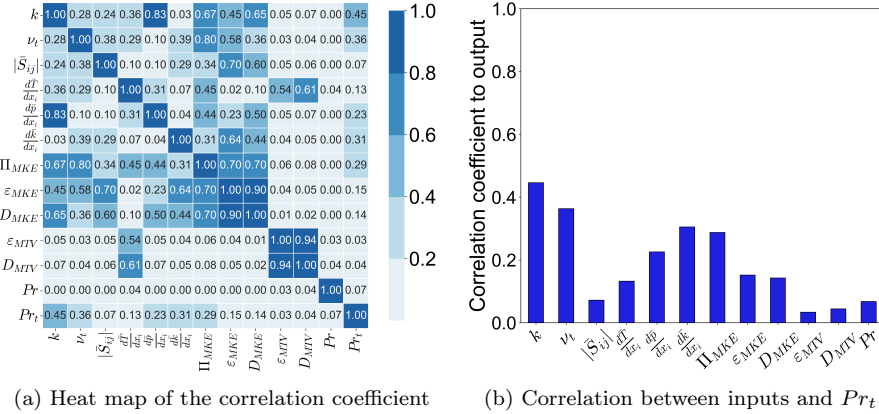


Figure 20: Pearson correlation coefficients of turbulent heat transfer in a duct.

## B. Training model and number of optimal parameters

To train ANNs efficiently for the database of  $Pr_t$ , the cosine annealing learning rate scheduler [78] and the ELU activation function [79] are used. The K-fold technique [63] with 5-fold cross validation [64] was used to minimize the overfitting issue. We select the number of the layers and neurons by a comparison study for hyper-parameters. Fig. 21 shows the RMSE values with the different values of the layer and neuron per layer. Each RMSE value is obtained from 120 trained ANNs. The error bars show 95% confidence intervals. The averaged RMSE show similar values over different conditions. We select 2 layers and 60 neurons/layer (2L-60N/L) based on relatively lower RMSE and better error bar range. To test dependency on the hyper-parameters, 1L-30N/L is also considered in the next section. Note



that all RMSE results are computed based on  $Pr_t^*$ . As  $\sigma_{Pr_t} = \sigma_Y = 0.334$ , 0.3 for the RMSE of  $Pr_t^*$  (as found in Fig. 21(b)) is equivalent to 0.1 for the RMSE of  $Pr_t$ .

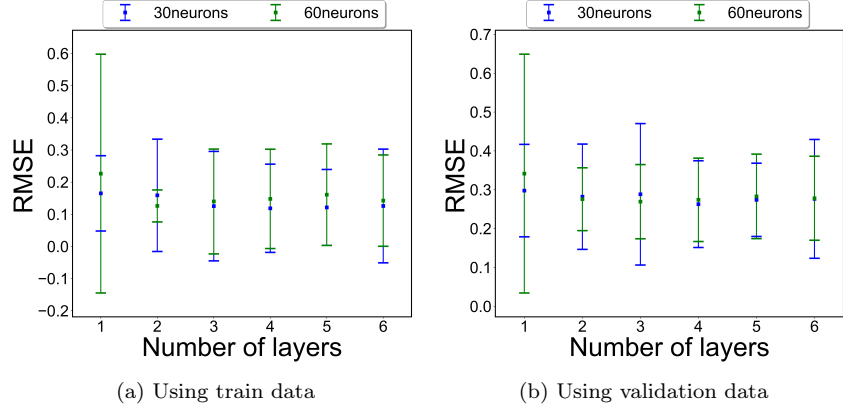


Figure 21: RMSE values with the different numbers of the layer and neuron per layer for turbulent heat transfer in a duct.

To estimate the dimension of a reduced  $Pr_t$  model, Fig. 22 shows the accumulated feature importance of the RF method and PCA over the number of components. The green line shows the RMSE of SGE-TD over the number of the input parameters. It is shown that RF needs 8-9 and PCA needs 5 parameters for sufficiently converged ( $> 90\%$  in importance) model prediction. The RMSE of SGE-TD decreases rapidly up to 4 parameters and fully converges from 6 parameters.

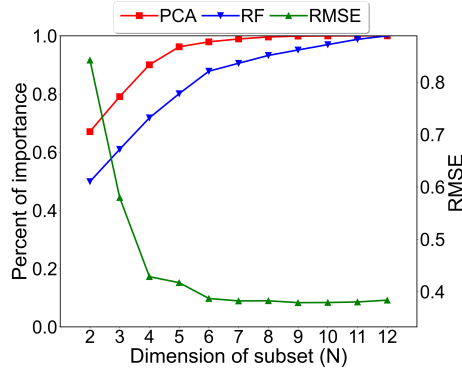


Figure 22: Accumulated feature importance of the RF method and PCA compared with the RMSE (validation) of SGE-TD over the number of components (including  $Pr$ ).

### C. Results of dimensionality reduction for $Pr_t$ model

The ANN-wrapper methods are applied to the full parameter  $Pr_t$  model. With respect to the trained ANNs, only the well-trained ANNs (50% below the RMSE median) are used.

Table IX shows PEM-CoT1 and PEM-CoT2 metrics of  $S_5$  and  $S_6$  over 60 selection trials of different methods. For brevity, the metrics were averaged over different hyper-parameters (1L-30N/L and 2L-60N/L). Note that  $Pr$  is an important global parameter for  $Pr_t$  and pre-included in the parameter subset. For both  $S_5$  and  $S_6$ , SGE-TD shows better CoT than the other methods, especially for PEM-CoT2 that shows at least 10% increase. Higher PEM-CoT2 of SGE-TD implies obtaining a specific parameter subset more stably. The second highest CoT is obtained by SBE. SGE-DC is a little behind SBE, followed by SFS by relatively large margins especially for PEM-CoT2.

Method	5-parameter subset ( $S_5$ )		6-parameter subset ( $S_6$ )	
	Average PEM-CoT1	Average PEM-CoT2	Average PEM-CoT1	Average PEM-CoT2
SFS	0.664	0.117	0.790	0.192
SBE	0.947	0.800	0.853	0.350
SGE-TD	0.973	0.892	0.877	0.425
SGE-DC	0.873	0.675	0.810	0.292

Table IX: PEM-CoT1 and PEM-CoT2 over 60 selection trials for turbulent heat transfer in a duct.

Table X show the list of 6 parameters with the highest selection possibilities from  $S_6$  over 60 selection trials. All methods include  $\nu_t$  and  $k$  with the exception to SFS. Notably, previously suggested two-equation models [80–83], which directly solves transport equations of the dissipation rate and thermal variance to modeling  $Pr_t$ , defines  $\alpha_t$  as a function of  $k$ , implying its importance in modeling  $Pr_t$ . With 2L-60N/L, the most selected parameters becomes identical between SGE and SBE methods. Note that the maximum inter-parameter correlation coefficients are shown to be smallest for the SGE methods followed by SBE and SFS. A lower maximum inter-parameter correlation may imply reduced overlapping effects.

Method	6 most selected parameters from $S_6$		Max. inter-parameter correlation	
	1L-30N/L	2L-60N/L	1L-30N/L	2L-60N/L
SFS	$\varepsilon_{MKE}, \varepsilon_{MTV}, \Pi_{MKE}, D_{MTV},  \partial\bar{P}/\partial x_i , Pr$	$\varepsilon_{MKE}, \varepsilon_{MTV}, \Pi_{MKE},  \bar{S}_{ij} ,  \partial\bar{P}/\partial x_i , Pr$	0.70	0.70
SBE	$\nu_t, k,  \partial T/\partial x_i , D_{MKE},  \bar{S}_{ij} , Pr$	$\nu_t, k,  \partial\bar{T}/\partial x_i ,  \partial k/\partial x_i , D_{MKE}, Pr$	0.60	0.54
SGE-TD	$\nu_t, k,  \partial T/\partial x_i , \varepsilon_{MTV}, D_{MKE}, Pr$	$\nu_t, k,  \partial\bar{T}/\partial x_i ,  \partial k/\partial x_i , D_{MKE}, Pr$	0.54	0.54
SGE-DC	$\nu_t, k,  \partial T/\partial x_i ,  \partial k/\partial x_i , D_{MKE}, Pr$	$\nu_t, k,  \partial\bar{T}/\partial x_i ,  \partial k/\partial x_i , D_{MKE}, Pr$	0.54	0.54

Table X: List of 6 parameters with the highest selection possibilities from  $S_6$  over 60 selection trials for turbulent heat transfer in a duct. Maximum inter-parameter correlation coefficients are shown in the right.

Fig. 23 shows the RMSE,  $J_{TD}$ , and  $J_{DC}$  averaged overs trials according to the size of the subset  $S_N$  for each method. Overall trends look similar to those of the previous applications. The RMSE is smallest for SFS and SBE by a relatively small margin, and  $J_{TD}$  and  $J_{DC}$  are smallest for the SGE methods. The RMSE shows that the reduced model converges with 5-6 parameters, similarly to the PCA result in Fig. 22.

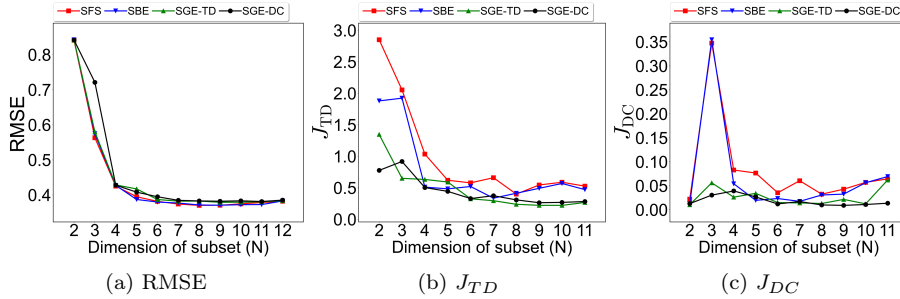


Figure 23: RMSE (validation),  $J_{TD}$ , and  $J_{DC}$  averaged overs trials according to the size of  $S_N$  for turbulent heat transfer in a duct (2L-60N/L).

Fig. 24 show the contours of  $Pr_t$  from the DNS, full parameter model, and reduced models ( $S_3$ ,  $S_6$ ,  $S_8$ , and  $S_{10}$ ) using SFS and SGE-TD. All models were trained for 60 times using the database of  $Pr=0.2$  and  $2.0$  without  $Pr=0.7$ . Then, the results for  $Pr=0.7$  predicted using the full parameter and reduced models are averaged over trained ANNs, in order to estimate the practical prediction accuracy with reduced training uncertainty. As expected,  $Pr_t$  using the full parameter model resembles the features of the DNS result most closely. The results of each reduced model

improve with the number of the parameters, but those using SFS show distorted streaks near the walls. SGE-TD, on the other hand, shows better prediction near the wall. SGE-TD shows superior prediction in the center region of the plot as well compared to SFS (particularly for  $S_3$ ). Even for  $S_3$ , SGE-TD shows higher resemblance with the DNS result while SFS completely fails to do so. It may also be emphasized that the effect of  $k$  is particularly important. Despite the fact that  $S_{10}$  of SFS and SGE-TD differ only by a single parameter ( $\varepsilon_{MTV}$  and  $k$ ),  $S_{10}$  with  $k$  (SGE-TD) predicts  $Pr_t$  better than the one without it.

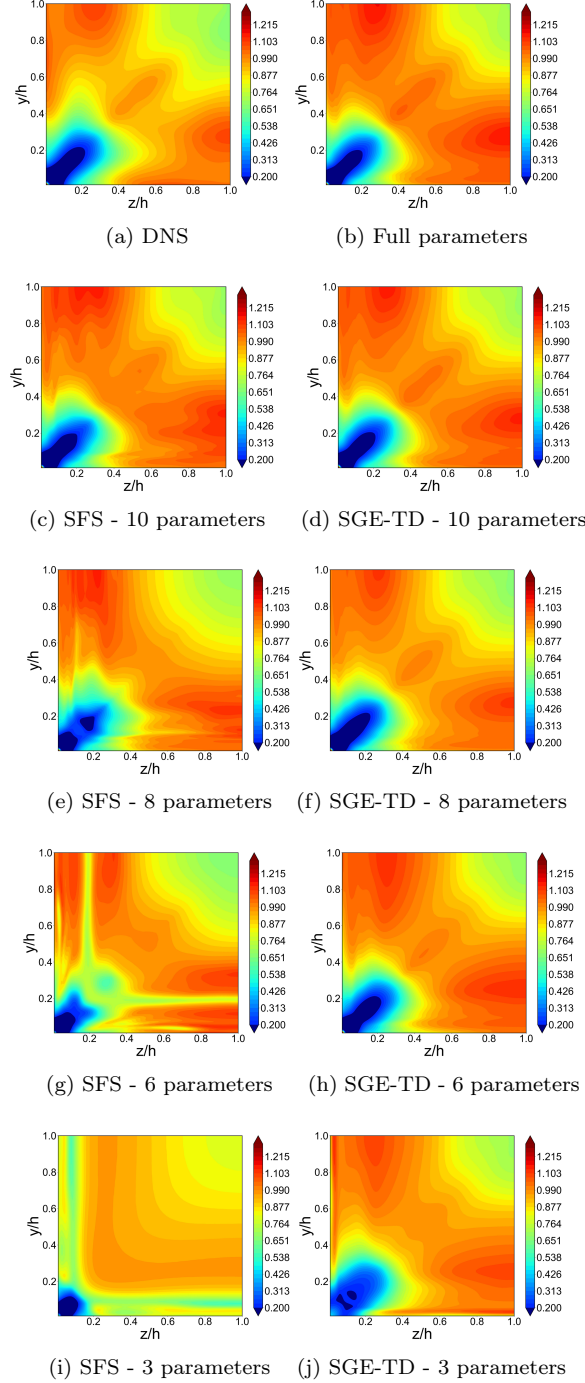


Figure 24: Contours of  $Pr_t$  from DNS, full parameter model, and reduced models ( $S_3$ ,  $S_6$ ,  $S_8$ , and  $S_{10}$ ) using SFS and SGE-TD for turbulent heat transfer in a duct with  $Pr = 0.7$  ( $2L-60N/L$ ). Only the left-bottom quadrant of the domain is shown.

To check the compatibility of the parameter subset between different hyper-parameters, Fig. 25 shows the RMSE of predicted  $Pr_t$  with 1L-30N/L using the subsets reduced with 2L-60N/L. Even when the reduced models are trained under lower hyper-parameters, SGE-TD is superior in the RMSE than SFS, although the difference decreases as the parameter dimension increases.

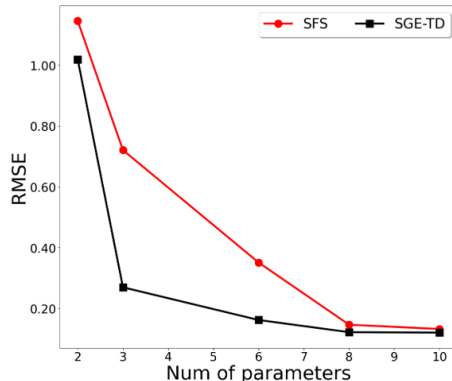


Figure 25: RMSE (validation) of predicted  $Pr_t$  with 1L-30N/L using the parameter subsets reduced with 2L-60N/L.

To examine the effects of different subsets from the wrapper methods on ANN training, Fig. 26 shows the RMSE with respect to epochs using  $S_6$  reduced with 1L-30N/L for three different hyper-parameters. SGE-TD has the lowest RMSE out of all methods. This shows relatively faster training speed, although the differences from the other methods are not very large except for SFS. SFS shows the highest RMSE value followed by SBE and SGE-DC.

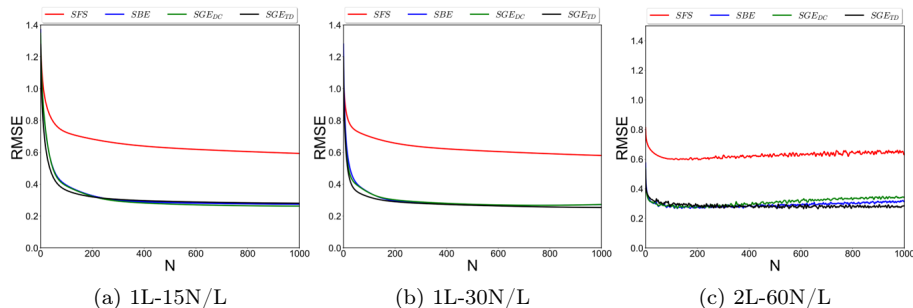


Figure 26: RMSE (validation) of  $S_6$  reduced with 1L-30N/L versus training epoch with different hyper-parameters for turbulent heat transfer in a duct. RMSEs are averaged over trials.

## VI. CONCLUSIONS

Data-driven modeling is an emerging topic of interest for their capability to reconstruct functional expressions of spatially distributed quantities derived from high-fidelity simulations and experiments. These databases, however, typically feature large number of related parameters and high non-linearity which often lead to inefficient and inaccurate training of the models. Thus, identification of primary parameters and systematic dimensionality reduction are of utmost importance, especially so in the field of turbulence modeling. In this study, ANN-based wrapper methods are analyzed and a novel approach is proposed to address a weakness of the existing methods. Due to the overfitting issue and random nature of ANN training, consistency of the parameter subsets over selection trials may be compromised especially in a high parameter dimension.

In order to relax this issue, we defined two performance evaluation metrics to evaluate consistency-over-trials (CoT) of the selected subsets. Also, novel subset selection indices were devised based on the gradient of the model function, under an idea that excessive weights from the overfitting distort the partial derivatives while reducing the RMSE. This leads to two sequential gradient-based elimination (SGE) methods that minimize the loss in the total derivative of reduced ANN models (SGE-TD) or the directional consistency of the gradient (SGE-DC) at each elimination step. A large RMSE in the trained ANN model leads to even larger error in its gradient, which can make the SGE selection

inconsistent. As a solution to this issue, it was found that SGE using the trained ANNs with relatively smaller RMSEs (50% below the average) can successfully remove redundant and irrelevant parameters. The training overhead could be minimized by using this approach only for the final subset. When this approach was applied to a manufactured subset selection problem, perfect success rates were achieved. To further evaluate the SGE methods, these and other existing ANN-wrapper methods (i.e., SFS and SBE) are tested for two turbulence modeling applications: bubbly flow in a pipe and heat transfer in a duct flow.

The ANN-wrapper methods were applied to the reduced modeling of the bubble size ( $D_{sm}$ ) in turbulent bubbly flows in a pipe. Using the results of experimental studies, a database for modeling  $D_{sm}$  was collected and the non-dimensional 5-parameter model of [46] is used as the full parameter model. Using SGE, the size of optimally reduced subset was smaller compared to the SFS (and RF) method and similar to the SBE method. Out of all the ANN-wrapper methods, only SFS selected  $J_G/J_L$  over  $\alpha_G$ , a well-known parameter for modeling  $D_{sm}$ . Rest of the methods selected nearly identical parameters. The CoT indices were also evaluated. SBE and SGE-TD showed ideal CoT for all cases. SGE-DC showed slightly low CoT with all trained ANNs but produced ideal CoT with well-trained ANNs. SFS showed relatively lower CoT than the others.

To analyze the ANN-wrapper methods for a higher-dimensional database, modeling  $Pr_t$  in a turbulent duct flow was considered to reduce a 12-parameter model composed of the physical parameters usually available from RANS simulations. The database was obtained from a DNS study. From the heat map of the correlation coefficients, complex relationships and the overlapping effects among the parameters were observed. As a result, SGE-TD showed the highest CoT indices followed by SBE, SGE-DC, and SFS in order. Higher CoT of SGE-TD was more pronounced for a higher-dimensional subset. Except for SFS showing relatively lower CoT and higher RMSE, all methods preferred selecting  $\nu_t$  and  $k$  for 6-parameter subsets. From the contours of  $Pr_t$  with different  $Pr$  from the training data, SGE-TD showed far superior prediction of  $Pr_t$  compared to SFS across all regions of the duct. Even for heavily reduced (3-parameter) subset, SGE-TD was relatively effective in  $Pr_t$  prediction. SFS, on the other hand, produced far inferior  $Pr_t$  prediction, which may further verify the importance of  $k$  and  $\nu_t$ . From a comparative study on the hyper-parameters and training speed, it was found that a reduced parameter subset is compatible among hyper-parameters, and SGE-TD showed the fastest training speed although the differences from the other methods are not very large.

In summary, the new ANN-wrapper method can successfully remove unnecessary parameters using only the gradient information, leading to optimal parameter subsets. Besides, more robust parameter selection with higher CoT compared to the existing methods can be achieved, which is useful for modeling physical problems with high-dimensional complexity using ANN.

## ACKNOWLEDGMENTS

This work was supported by the National Research Foundation of Korea (NRF) grants funded by the Korea government (MSIP) (No. 2017M2A8A4018482, 2017R1A2B3008273, and 2022R1F1A1074931).

## APPENDIX. THE BUDGET EQUATIONS FOR KINETIC AND THERMAL ENERGY IN TURBULENT FLOWS

From the theories on turbulent flows, the budgets of the TKE ( $k = \frac{1}{2}\overline{u'_j u'_j}$ ) and temperature variance (TV,  $\overline{T' T'}$ ) have been considered for an analysis of the energy transfer by fluctuation components. Similarly, the budgets for the mean kinetic energy (MKE) and mean temperature variance (MTV) are considered. Their governing equations are written as

$$\underbrace{\frac{1}{2} \frac{D\overline{u_j u_j}}{Dt}}_{SD_{MKE}} = \underbrace{-\frac{\partial \overline{u_i u'_i u'_j}}{\partial x_j}}_{C_{MKE}} + \underbrace{2\nu \frac{\partial \overline{u_i S_{ij}}}{\partial x_j}}_{D_{MKE}} - \underbrace{\frac{1}{\rho} \frac{\partial \overline{u_j \overline{p}}}{\partial x_j}}_{\Pi_{MKE}} + \underbrace{\overline{u'_i u'_j} \frac{\partial \overline{u_i}}{\partial x_j}}_{-P_{TKE}} - \underbrace{2\nu \overline{S_{ij} S_{ij}}}_{\varepsilon_{MKE}}, \quad (23)$$

$$\underbrace{\frac{1}{2} \frac{D\overline{T T}}{Dt}}_{SD_{MTV}} = \underbrace{-\frac{\partial \overline{T u'_j T'}}{\partial x_j}}_{A_{MTV}} + \underbrace{\frac{\alpha}{2} \frac{\partial^2 \overline{T T}}{\partial x_j \partial x_j}}_{D_{MTV}} + \underbrace{\overline{T' u'_j} \frac{\partial \overline{T}}{\partial x_j}}_{-P_{TV}} - \underbrace{\alpha \frac{\partial \overline{T}}{\partial x_j} \frac{\partial \overline{T}}{\partial x_j}}_{\varepsilon_{MTV}}. \quad (24)$$

where  $S_{ij}$  denotes the strain rate tensor. The overbar ( $\overline{\quad}$ ) and prime ( $'$ ) symbols denote averaged and fluctuation components of a variable, respectively. The term  $\varepsilon_{MKE}$  and  $\varepsilon_{MTV}$  denote the MKE dissipation and MTV dissipation,

respectively.

- 
- [1] K. Duraisamy, G. Iaccarino, H. Xiao, Turbulence modeling in the age of data, *Annual Review of Fluid Mechanics* 51 (2019) 357–377. doi:doi:10.1146/annurev-fluid-010518-040547.
- [2] S. L. Brunton, B. R. Noack, P. Koumoutsakos, Machine learning for fluid mechanics, *Annual review of fluid mechanics* 52 (2020) 477–508. doi:doi:10.1146/annurev-fluid-010719-060214.
- [3] R. Vinuesa, S. L. Brunton, Enhancing computational fluid dynamics with machine learning, *Nature Computational Science* 2 (2022) 358–366. doi:doi:10.1038/s43588-022-00264-7.
- [4] M. Milano, P. Koumoutsakos, Neural network modeling for near wall turbulent flow, *Journal of Computational Physics* 182 (2002) 1–26. doi:doi:10.1006/jcph.2002.7146.
- [5] Y. Bin, L. Chen, G. Huang, X. I. A. Yang, Progressive, extrapolative machine learning for near-wall turbulence modeling, *Physical Review Fluids* 7 (2022) 084610. doi:doi:10.1103/physrevfluids.7.084610.
- [6] F. Sarghini, G. De Felice, S. Santini, Neural networks based subgrid scale modeling in large eddy simulations, *Computers & fluids* 32 (2003) 97–108. doi:doi:10.1016/s0045-7930(01)00098-6.
- [7] A. Subel, A. Chattopadhyay, Y. Guan, P. Hassanzadeh, Data-driven subgrid-scale modeling of forced burgers turbulence using deep learning with generalization to higher reynolds numbers via transfer learning, *Physics of Fluids* 33 (2021) 031702. doi:doi:10.1063/5.0040286.
- [8] J. Ling, A. Kurzawski, J. Templeton, Reynolds averaged turbulence modelling using deep neural networks with embedded invariance, *Journal of Fluid Mechanics* 807 (2016) 155–166. doi:doi:10.1017/jfm.2016.615.
- [9] B. D. Tracey, K. Duraisamy, J. J. Alonso, A machine learning strategy to assist turbulence model development, in: 53rd AIAA Aerospace Sciences Meeting, American Institute of Aeronautics and Astronautics, 2015. doi:doi:10.2514/6.2015-1287.
- [10] P. S. Volpiani, M. Meyer, L. Franceschini, J. Dandois, F. Renac, E. Martin, O. Marquet, D. Sipp, Machine learning-augmented turbulence modeling for rans simulations of massively separated flows, *Physical Review Fluids* 6 (2021) 064607. doi:doi:10.1103/physrevfluids.6.064607.
- [11] A. Janecek, W. Gansterer, M. Demel, G. Ecker, On the relationship between feature selection and classification accuracy, in: Y. Saeyns, H. Liu, I. Inza, L. Wehenkel, Y. V. de Pee (Eds.), *Proceedings of the Workshop on New Challenges for Feature Selection in Data Mining and Knowledge Discovery at ECML/PKDD 2008*, volume 4 of *Proceedings of Machine Learning Research*, PMLR, Antwerp, Belgium, 2008, pp. 90–105. URL: <http://proceedings.mlr.press/v4/janecek08a.html>.
- [12] L. Ladha, T. Deepa, Feature selection methods and algorithms, *International Journal on Computer Science and Engineering* 3 (2011) 1787–1797.
- [13] S. Marsland, *Machine Learning: An Algorithmic Perspective*, 1st ed., Chapman & Hall/CRC, 2009. doi:doi:10.1201/b17476.
- [14] G. James, D. Witten, T. Hastie, R. Tibshirani, *An Introduction to Statistical Learning*, Springer New York, 2013. doi:doi:10.1007/978-1-4614-7138-7.
- [15] Z. J. Zhang, K. Duraisamy, Machine learning methods for data-driven turbulence modeling, in: 22nd AIAA Computational Fluid Dynamics Conference, American Institute of Aeronautics and Astronautics, 2015. doi:doi:10.2514/6.2015-2460.
- [16] K. Duraisamy, Z. J. Zhang, A. P. Singh, New approaches in turbulence and transition modeling using data-driven techniques, in: 53rd AIAA Aerospace Sciences Meeting, American Institute of Aeronautics and Astronautics, 2015. doi:doi:10.2514/6.2015-1284.
- [17] E. J. Parish, K. Duraisamy, A paradigm for data-driven predictive modeling using field inversion and machine learning, *Journal of Computational Physics* 305 (2016) 758–774. doi:doi:10.1016/j.jcp.2015.11.012.
- [18] L. Sun, W. An, X. Liu, H. Lyu, On developing data-driven turbulence model for dg solution of rans, *Chinese Journal of Aeronautics* 32 (2019) 1869–1884. doi:doi:10.1016/j.cja.2019.04.004.
- [19] A. A. Moghaddam, A. Sadaghiyani, A deep learning framework for turbulence modeling using data assimilation and feature extraction, *arXiv preprint arXiv:1802.06106* (2018).
- [20] B. J. Isaac, A. Coussement, O. Gicquel, P. J. Smith, A. Parente, Reduced-order pca models for chemical reacting flows, *Combustion and flame* 161 (2014) 2785–2800. doi:doi:10.1016/j.combustflame.2014.05.011.
- [21] S. Khalid, T. Khalil, S. Nasreen, A survey of feature selection and feature extraction techniques in machine learning, in: 2014 Science and Information Conference, IEEE, 2014. doi:doi:10.1109/sai.2014.6918213.
- [22] J. Liu, S. Ji, J. Ye, Multi-task feature learning via efficient l<sub>2,1</sub>-norm minimization, in: *Proceedings of the twenty-fifth conference on uncertainty in artificial intelligence*, AUAI Press, 2009, pp. 339–348.
- [23] Z. Zhao, L. Wang, H. Liu, Efficient spectral feature selection with minimum redundancy, in: *Twenty-fourth AAAI conference on artificial intelligence*, 2010. doi:doi:10.1609/aaai.v24i1.7671.
- [24] M. A. Kramer, Nonlinear principal component analysis using autoassociative neural networks, *AICHe journal* 37 (1991) 233–243. doi:doi:10.1002/aic.690370209.
- [25] H. Mirgolbabaei, T. Echehki, N. Smaoui, A nonlinear principal component analysis approach for turbulent combustion composition space, *international journal of hydrogen energy* 39 (2014) 4622–4633. doi:doi:10.1016/j.ijhydene.2013.12.195.
- [26] J. L. Callahan, J. V. Koch, B. W. Brunton, J. N. Kutz, S. L. Brunton, Learning dominant physical processes with data-driven balance models, *Nature communications* 12 (2021) 1–10. doi:doi:10.26226/morressier.612f6736bc98103724100896.
- [27] I. Guyon, A. Elisseeff, An introduction to variable and feature selection, *Journal of Machine Learning Research* 3 (2003) 1157–1182.

- [28] S. Biswas, M. Bordoloi, B. Purkayastha, Review on feature selection and classification using neuro-fuzzy approaches, *International Journal of Applied Evolutionary Computation* 7 (2016) 28–44. doi:doi:10.4018/ijaec.2016100102.
- [29] G. Chandrashekar, F. Sahin, A survey on feature selection methods, *Computers & Electrical Engineering* 40 (2014) 16–28. doi:doi:10.1016/j.compeleceng.2013.11.024.
- [30] C.-W. Chang, N. T. Dinh, Classification of machine learning frameworks for data-driven thermal fluid models, *International Journal of Thermal Sciences* 135 (2019) 559–579. doi:doi:10.1016/j.ijthermalsci.2018.09.002.
- [31] D. P. Kingma, J. Ba, Adam: A method for stochastic optimization, *ArXiv* (2014). [arXiv:1412.6980](https://arxiv.org/abs/1412.6980).
- [32] G. H. John, R. Kohavi, K. Pfleger, Irrelevant features and the subset selection problem, in: *Machine Learning Proceedings 1994*, Elsevier, 1994, pp. 121–129. doi:doi:10.1016/b978-1-55860-335-6.50023-4.
- [33] R. Kohavi, G. H. John, Wrappers for feature subset selection, *Artificial Intelligence* 97 (1997) 273–324. doi:doi:10.1016/s0004-3702(97)00043-x.
- [34] A. Marcano-Cedeno, J. Quintanilla-Domínguez, M. G. Cortina-Januchs, D. Andina, Feature selection using sequential forward selection and classification applying artificial metaplasticity neural network, in: *IECON 2010-36th annual conference on IEEE industrial electronics society, IEEE*, 2010, pp. 2845–2850. doi:doi:10.1109/iecon.2010.5675075.
- [35] L. C. Molina, L. Belanche, A. Nebot, Feature selection algorithms: a survey and experimental evaluation, in: *2002 IEEE International Conference on Data Mining Proceedings, IEEE Comput. Soc*, 2002. doi:doi:10.1109/icdm.2002.1183917.
- [36] I. A. Gheyas, L. S. Smith, Feature subset selection in large dimensionality domains, *Pattern Recognition* 43 (2010) 5–13. doi:doi:10.1016/j.patcog.2009.06.009.
- [37] I. E. Thambi, R. Anju, R. Rajan, An extensive study on data thinning in single and ensemble classifiers, *International Journal of Pure and Applied Mathematics* 114 (2017) 1–9.
- [38] L. Yu, H. Liu, Efficient feature selection via analysis of relevance and redundancy, *Journal of Machine Learning Research* 5 (2004) 1205–1224.
- [39] M. Colombo, M. Fairweather, Multiphase turbulence in bubbly flows: RANS simulations, *International Journal of Multiphase Flow* 77 (2015) 222–243. doi:doi:10.1016/j.ijmultiphaseflow.2015.09.003.
- [40] M. Ishii, K. Mishima, Two-fluid model and hydrodynamic constitutive relations, *Nuclear Engineering and Design* 82 (1984) 107–126. doi:doi:10.1016/0029-5493(84)90207-3.
- [41] B. J. Kim, J. Kim, K. D. Kim, On the wall drag term in the averaged momentum equation for dispersed flows, *Nuclear Science and Engineering* 178 (2014) 225–239. doi:doi:10.13182/nse13-57.
- [42] M. Ishii, N. Zuber, Drag coefficient and relative velocity in bubbly, droplet or particulate flows, *AIChE Journal* 25 (1979) 843–855. doi:doi:10.1002/aic.690250513.
- [43] Y. Sato, M. Sadatomi, K. Sekoguchi, Momentum and heat transfer in two-phase bubble flow-I. Theory, *International Journal of Multiphase Flow* 7 (1981) 167–177. doi:doi:10.1016/0301-9322(81)90003-3.
- [44] A. Tomiyama, H. Tamai, I. Zun, S. Hosokawa, Transverse migration of single bubbles in simple shear flows, *Chemical Engineering Science* 57 (2002) 1849–1858. doi:doi:10.1016/s0009-2509(02)00085-4.
- [45] Y.-D. Kim, E. Park, S. Yoo, T. Choi, L. Yang, D. Shin, Compression of deep convolutional neural networks for fast and low power mobile applications, *arXiv preprint arXiv:1511.06530* (2015).
- [46] H. Jung, S. Yoon, Y. Kim, J. H. Lee, H. Park, D. Kim, J. Kim, S. Kang, Development and evaluation of data-driven modeling for bubble size in turbulent air-water bubbly flows using artificial multi-layer neural networks, *Chemical Engineering Science* (2019) 115357. doi:doi:10.1016/j.ces.2019.115357.
- [47] M. Colombo, M. Fairweather, Accuracy of Eulerian–Eulerian, two-fluid CFD boiling models of subcooled boiling flows, *International Journal of Heat and Mass Transfer* 103 (2016) 28–44. doi:doi:10.1016/j.ijheatmasstransfer.2016.06.098.
- [48] T. Hibiki, M. Ishii, One-group interfacial area transport of bubbly flows in vertical round tubes, *International Journal of Heat and Mass Transfer* 43 (2000) 2711–2726. doi:doi:10.1016/s0017-9310(99)00325-7.
- [49] T. Hibiki, M. Ishii, Interfacial area concentration of bubbly flow systems, *Chemical Engineering Science* 57 (2002) 3967–3977. doi:doi:10.1016/s0009-2509(02)00263-4.
- [50] S. C. P. Cheung, G. H. Yeoh, J. Y. Tu, On the numerical study of isothermal vertical bubbly flow using two population balance approaches, *Chemical Engineering Science* 62 (2007) 4659–4674. doi:doi:10.1016/j.ces.2007.05.030.
- [51] S. Lo, A. Splawski, B. J. Yun, The importance of correct modeling of bubble size and condensation in prediction of subcooled boiling flows, *The Journal of Computational Multiphase Flows* 4 (2012) 299–308. doi:doi:10.1260/1757-482x.4.3.299.
- [52] V.-T. Nguyen, B.-U. Bae, D.-J. Euh, C.-H. Song, B.-J. Yun, The effect of bubble-induced turbulence on the interfacial area transport in gas-liquid two-phase flow, *The Journal of Computational Multiphase Flows* 4 (2012) 327–340. doi:doi:10.1260/1757-482x.4.3.327.
- [53] C.-H. Lin, T. Hibiki, Databases of interfacial area concentration in gas-liquid two-phase flow, *Progress in Nuclear Energy* 74 (2014) 91–102. doi:doi:10.1016/j.pnucene.2014.01.015.
- [54] T.-J. Chuang, T. Hibiki, Vertical upward two-phase flow CFD using interfacial area transport equation, *Progress in Nuclear Energy* 85 (2015) 415–427. doi:doi:10.1016/j.pnucene.2015.07.008.
- [55] J. P. Schlegel, T. Hibiki, A correlation for interfacial area concentration in high void fraction flows in large diameter channels, *Chemical Engineering Science* 131 (2015) 172–186. doi:doi:10.1016/j.ces.2015.04.004.
- [56] Y. Liao, R. Rzehak, D. Lucas, E. Krepper, Baseline closure model for dispersed bubbly flow: Bubble coalescence and breakup, *Chemical Engineering Science* 122 (2015) 336–349. doi:doi:10.1016/j.ces.2014.09.042.
- [57] A. Shaikh, M. Al-Dahhan, Development of an artificial neural network correlation for prediction of overall gas holdup in bubble column reactors, *Chemical Engineering and Processing: Process Intensification* 42 (2003) 599–610. doi:doi:10.1016/s0255-2701(02)00209-x.

- [58] G. Monrós-Andreu, S. Chiva, R. Martínez-Cuenca, S. Torró, J. E. Juliá, L. Hernández, R. Mondragón, Water temperature effect on upward air-water flow in a vertical pipe: Local measurements database using four-sensor conductivity probes and LDA, in: EPJ Web of Conferences, volume 45, EDP Sciences, 2013, p. 01105. doi:doi:10.1051/epjconf/20134501105.
- [59] M. Ma, J. Lu, G. Tryggvason, Using statistical learning to close two-fluid multiphase flow equations for bubbly flows in vertical channels, *International Journal of Multiphase Flow* 85 (2016) 336–347. doi:doi:10.1016/j.ijmultiphaseflow.2016.06.021.
- [60] T. Hibiki, S. Hogsett, M. Ishii, Local measurement of interfacial area, interfacial velocity and liquid turbulence in two-phase flow, *Nuclear Engineering and Design* 184 (1998) 287–304. doi:doi:10.1016/s0029-5493(98)00203-9.
- [61] T. Hibiki, M. Ishii, Z. Xiao, Axial interfacial area transport of vertical bubbly flows, *International Journal of Heat and Mass Transfer* 44 (2001) 1869–1888. doi:doi:10.1016/s0017-9310(00)00232-5.
- [62] B. Doup, X. Zhou, X. Sun, Local gas and liquid parameter measurements in air-water two-phase flows, *Nuclear Engineering and Design* 263 (2013) 273–283. doi:doi:10.1016/j.nucengdes.2013.05.022.
- [63] L. Breiman, P. Spector, Submodel selection and evaluation in regression. the X-random case, *International statistical review/revue internationale de Statistique* (1992) 291–319. doi:doi:10.2307/1403680.
- [64] R. Kohavi, A study of cross-validation and bootstrap for accuracy estimation and model selection, in: *Proceedings of the 14th International Joint Conference on Artificial Intelligence - Volume 2, IJCAI'95*, Morgan Kaufmann Publishers Inc., San Francisco, CA, USA, 1995, pp. 1137–1143.
- [65] A. J. Reynolds, The prediction of turbulent Prandtl and Schmidt numbers, *International Journal of Heat and Mass Transfer* 18 (1975) 1055–1069. doi:doi:10.1016/0017-9310(75)90223-9.
- [66] R. A. Antonia, L. W. B. Browne, Convective and conditional Prandtl number in a turbulent plane wake, *International Journal of Heat and Mass Transfer* 30 (1987) 2023–2030. doi:doi:10.1016/0017-9310(87)90083-4.
- [67] Y. Zhou, R. M. C. So, M. H. Liu, H. J. Zhang, Complex turbulent wakes generated by two and three side-by-side cylinders, *International Journal of Heat and Fluid Flow* 21 (2000) 125–133. doi:doi:10.1016/s0142-727x(99)00077-6.
- [68] G. Xu, Y. Zhou, Momentum and heat transfer in a turbulent cylinder wake behind a streamwise oscillating cylinder, *International Journal of Heat and Mass Transfer* 48 (2005) 4062–4072. doi:doi:10.1016/j.ijheatmasstransfer.2005.04.029.
- [69] L. P. Chua, R. A. Antonia, Turbulent Prandtl number in a circular jet, *International Journal of Heat and Mass Transfer* 33 (1990) 331–339. doi:doi:10.1016/0017-9310(90)90102-z.
- [70] L. P. Chua, Y. F. Li, T. Zhou, C. M. S. Yu, Measurements of turbulent Prandtl number of a heated square jet, *Measurements* 10 (2001) 14.
- [71] R. G. Deissler, Analysis of fully developed turbulent heat transfer at low Peclet numbers in smooth tubes with application to liquid metals, *NACA Research Memorandum E52F05* (1952).
- [72] S. Aoki, A consideration on the heat transfer in liquid metal, *Bulletin of the Tokyo Institute of Technology* 54 (1963) 63–73.
- [73] M. Jischa, H. B. Rieke, About the prediction of turbulent Prandtl and Schmidt numbers from modeled transport equations, *International Journal of Heat and Mass Transfer* 22 (1979) 1547–1555. doi:doi:10.1016/0017-9310(79)90134-0.
- [74] C. Rosén, C. Trägrdh, Prediction of turbulent high Schmidt number mass transfer using a low Reynolds number  $k-\epsilon$  turbulence model, *The Chemical Engineering Journal and the Biochemical Engineering Journal* 59 (1995) 153–159. doi:doi:10.1016/0923-0467(94)02921-0.
- [75] W. M. Kays, Turbulent Prandtl number—Where are we?, *Journal of Heat Transfer* 116 (1994) 284–295. doi:doi:10.1115/1.2911398.
- [76] G. Tang, H. Shi, Y. Wu, J. Lu, Z. Li, Q. Liu, H. Zhang, A variable turbulent Prandtl number model for simulating supercritical pressure CO<sub>2</sub> heat transfer, *International Journal of Heat and Mass Transfer* 102 (2016) 1082–1092. doi:doi:10.1016/j.ijheatmasstransfer.2016.06.046.
- [77] S. Nam, Effects of spatially non-uniform wall temperature on turbulent heat transfer inside a square duct, Master's thesis, Sogang University, 2022.
- [78] I. Loshchilov, F. Hutter, Sgdr: Stochastic gradient descent with warm restarts, arXiv preprint arXiv:1608.03983 (2016).
- [79] D.-A. Clevert, T. Unterthiner, S. Hochreiter, Fast and accurate deep network learning by exponential linear units (elus), arXiv preprint arXiv:1511.07289 (2015).
- [80] K. Abe, T. Kondoh, Y. Nagano, A new turbulence model for predicting fluid flow and heat transfer in separating and reattaching flows—II. thermal field calculations, *International Journal of Heat and Mass Transfer* 38 (1995) 1467–1481. doi:doi:10.1016/0017-9310(94)00252-q.
- [81] K. W. Brinckman, W. H. Calhoun, S. M. Dash, Scalar fluctuation modeling for high-speed aeropropulsive flows, *AIAA Journal* 45 (2007) 1036–1046. doi:doi:10.2514/1.21075.
- [82] T. P. Sommer, R. M. C. So, H. S. Zhang, Near-wall variable-prandtl-number turbulence model for compressible flows, *AIAA Journal* 31 (1993) 27–35. doi:doi:10.2514/3.11314.
- [83] B. Deng, W. Wu, S. Xi, A near-wall two-equation heat transfer model for wall turbulent flows, *International Journal of Heat and Mass Transfer* 44 (2001) 691–698. doi:doi:10.1016/s0017-9310(00)00131-9.